Published in final edited form as:
J Am Chem Soc. 2009 June 10; 131(22): 7869–7878. doi:10.1021/ja901868q.

S K-edge XAS and DFT Calculations on Cytochrome P450: Covalent and Ionic Contributions to the Cysteine-Fe Bond and Their Contribution to Reactivity

Abhishek Dey[+], **Yonging Jiang**[#], **Paul Ortiz de Montellano**[#,*], **Keith O. Hodgson**[+,±,*], **Britt Hedman**[±,*], and **Edward I. Solomon**[+,±,*]

[+] Department of Chemistry, Stanford University, Stanford, CA, 94305

[±] Stanford Synchrotron Radiation Lightsource, SLAC, Stanford University, Menlo Park, California 94025

[#] Department of Pharmaceutical Chemistry, University of California, San Francisco, CA, 94158

Abstract

Experimental covalencies of the Fe-S bond for the resting low-spin and substrate-bound high-spin active site of cytochrome P450 are reported. DFT calculations on the active site indicate that one H-bonding interaction from the protein backbone is needed to reproduce the experimental values. The H-bonding to the thiolate from the backbone decreases the anisotropic π covalency of the Fe-S bond lowering the barrier of free rotation of the exchangeable axial ligand, which is important for reactivity. The anionic axial thiolate ligand is calculated to lower the $Fe^{III/II}$ reduction potential of the active site by more than 1 V compared to a neutral imidazole ligand. About half of this derives from its covalent bonding and half from its electrostatic interaction with the oxidized Fe. This axial thiolate ligand increases the pKa of compound 0 (Fe^{III}-hydroperoxo) favoring its protonation which promotes O-O bond heterolysis forming compound I. The reactivity of compound I is calculated to be relatively insensitive to the nature of the axial ligand due to opposing reduction potential and proton affinity contributions to the H-atom abstraction energy.

Keywords

Cytochrome P450; S K-edge XAS; DFT; H-bonding

Introduction

Cytochrome P450's are involved in a number of critical processes in biology that use molecular oxygen to oxidize a large range of substrates in all forms of life.[1,2] The presence of an axial thiolate ligand distinguishes these enzymes from other heme-based oxygenases and oxidases.[3] One of the most well-studied members of this family is cytochrome P450cam from *Pseudomonas putida*. At room temperature the resting ferric state is low-spin which upon substrate (camphor) binding becomes high-spin.[4,5] This change of spin state increases the reduction potential of this active site by +125 mV, enabling its reduction.[4]

CORRESPONDING AUTHOR FOOTNOTE: all correspondence should be addressed to Edward.Solomon@stanford.edu.

Supporting Information Available. The optimized co-ordinates of the models and the full reference for Gaussian 03 are available at the World Wide Web at http://pubs.acs.org.

The mechanisms of O_2 activation and C-H bond hydroxylation have been discussed in great detail in many review articles.[1,2,6,7] O_2 binds to the substrate-bound ferrous active site and forms an oxy-adduct that is then reduced by another electron and protonated to generate a ferric hydroperoxy species, referred to as compound 0. This species then undergoes a proton-assisted heterolytic cleavage of the O-O bond, generating a high-valent species, compound I, that is mostly considered to be an Fe(IV)=O with a porphyrin monoanion radical. This has been identified as the primary oxidant in the reaction mechanism, which does an H-atom abstraction that generates an Fe^{IV}-OH species and a substrate radical. This is followed by hydroxyl rebound, which results in a hydroxylated substrate and a ferric resting site. Several key residues have been identified in the active site of P450 that play important roles in its reactivity. Particularly, threonine-252 has been implicated in the proton transfer pathway for the reaction, and mutation of this residue leads to loss of monooxygenase reactivity and uncoupled production of H_2O_2.[8,9]

The axial thiolate ligand has been proposed to provide a “push effect” that drives O-O bond heterolysis in the absence of a “pull-effect” from strong H-bonding residues present in the distal pocket of non-thiolate ligated heme peroxidases.[7] This push effect is generally proposed to play two roles. First, it increases electron density on the iron in the ferric state that weakens the binding of any exogenous ligand i.e. a normal trans effect associated with a strong donor.[10] Second, this push-effect is also proposed to weaken the O-O bond, activating it for heterolytic cleavage.[11] The first effect has experimental evidence (vis-à-vis weak exogenous axial ligand affinity).[10] However, the latter, and other effects that the Fe-S bond may have on the reaction cycle of P450, have been a focus of many studies and still lack consensus. Further, there is a highly conserved H-bonding interaction to the S atom of this thiolate that is proposed to be important for reactivity.[12] However the role of the H-bond in tuning the Fe-S bond and its push effect are not clear from the results of conventional spectroscopic techniques. Sulfur K-edge X-ray absorption spectroscopy (XAS) is a powerful physical method that provides a direct experimental estimate of the covalency of metal-ligand bonds.[13,14] The K-edge spectrum of a ligand bound to a transition metal can have an intense *pre-edge* feature. This is assigned to the ligand 1s (L_{1s}) to metal 3d (M_{3d}) transition. The intensity of this transition (i.e. I ($L_{1s} \rightarrow M_{3d}$) in eq. 2, below) is directly proportional to the % ligand np character (α^2) mixed into unoccupied or half-occupied orbitals of the ground state wavefunction (Ψ, eq. 1) of the transition metal complex.[15]

$$\Psi=(1-\alpha^2)^{1/2}|M_{3d}> - \alpha|L_{np}> \quad (1)$$

$$I(L_{1s} \rightarrow M_{3d})=\alpha^2 I(L_{1s} \rightarrow L_{np}) \quad (2)$$

$I(S_{1s} \rightarrow S_{np})$ is the intensity of a purely ligand-based 1s→ np transition, which depends primarily on the Z_{eff} of the ligand.[15] The pre-edge intensity thus provides a direct estimate of ligand-metal bond covalency (α^2).

S K-edge XAS has previously been used to investigate the effect of H-bonding in the active sites of Fe-S electron transfer proteins.[14] XAS data on the proteins showed significant reductions of M-S bond covalency relative to model complexes which qualitatively correlated to the H-bonding interactions in the active site.[16–18] For a quantitative estimate of this effect, S K-edge XAS was performed on a series of high-spin ferric heme thiolate model complexes where the H-bonding to the thiolate ligand was systematically varied from 0 to 2 H-bonds.[19]

The data showed dramatic reduction in pre-edge intensity with increasing H-bonding which indicated weakening of Fe-S d-π bond covalency.

In this study we use a combination of S K-edge XAS and DFT calculations to understand the nature of the Fe-S bond at the active site of cytochrome P450 in its resting low-spin and substrate bound high-spin states. The experimentally calibrated computational results further explore the role of the thiolate ligand and H-bonding to the thiolate sulfur at different steps of the reaction cycle.

Experimental Details

Materials and Methods

Cytochrome P450cam was purified after heterologous expression in *E. coli* as previously described.[20] The resting oxidized (Fe^{III}) (100 mM phosphate at pH 7.0) and substrate bound (100 mM phosphate, 200 mM KCl, 3 equivalents of camphor at pH = 7.0) protein solutions were loaded via a syringe into a Pt-plated Al block sample holder sealed in front using a 6.3 μm polypropylene window and maintained at a constant temperature of 24 °C during data collection using a controlled flow of N_2 gas pre-cooled by liq. N_2 passing through an internal channel in the Al block. Conversion to the substrate-bound form was monitored by an absorption feature at 387 nm and found to be > 99% in the high-spin Fe^{III} state.

Data Collection

XAS data were measured at the Stanford Synchrotron Radiation Lightsource using the 54-pole wiggler beam line 6–2. Details of the experimental configuration for low energy studies have been described previously.[14] The energy calibration, data reduction and error analysis follow the methods in the literature.[21]

Fitting Procedures

Pre-edge features were fit by pseudo-Voigt line shapes (sums of Lorentzian and Gaussian functions) using the EDG_FIT software.[22] This line shape is appropriate as the experimental features are a convolution of a Lorentzian transition envelope and a Gaussian line shape imposed by the beam line optics.[23,24] A fixed 1:1 ratio of Lorentzian to Gaussian contribution successfully reproduced the pre-edge features. The rising edges were also fit with pseudo-Voigt line shapes. Fitting requirements included reproducing the data and its second derivative, using the minimum number of peaks. The intensity of a pre-edge feature (peak area) was calculated as 2 × amplitude × fwhm, where fwhm is the full-width-at-half-maximum (between 0.45–0.5 for each peak). The fitted intensities were converted to $\%S_{3p}$ character using the pre-edge feature of plastocyanin as a reference (where 1.01 units of intensity, obtained using EDG_FIT, corresponded to 38% S_{3p} character) as the Z_{eff} on the S atom of the thiolate ligand will not change significantly between the Cu-SCys active site of plastocyanin and the Fe-SCys active site in P450.

DFT Calculations

All optimizations were performed using a 6-311g* basis set for Fe, S, N and O atoms and a 6-31g* basis set for C and H atoms in the Gaussian 03 program ver. C02[25] employing the BP86[26,27] functional and the B3LYP[28,29] hybrid functional. Single point calculations were performed using the B3LYP functional and a 6-311+g* basis set in the gas phase for wavefunctions and in a PCM[30] with an ε=4.0 was used for energies. The molecular orbitals were plotted using Gaussview ver. 3 and Mulliken[31] population analyses were performed using the PyMOlyze[32] program. The coordinates for the geometry optimization were obtained from the high resolution crystal structure 1dz4.[33]

1. Results and Analysis

A. XAS

The S K-edge XAS data for the substrate (camphor) bound high-spin P450 has an intense pre-edge feature at 2470.07 eV (Fig. 1, red). Contributions from the transitions to the three half-occupied t_2 orbitals and two half-occupied e orbitals are not resolved due to the low 10Dq for the high spin state. The pre-edge intensity is 1.11 ± 0.03 units (Table 1, 1st row) which corresponds to 41 ± 1% S_{3p} mixing into the unoccupied Fe_{3d} orbitals (; Table 1, 1st row in bold), i.e. covalency (using the value of $I(L_{1s} \rightarrow L_{3p})$ of plastocyanin in equation 2).[14] In our previous study, the Fe-S bond covalency for a five co-ordinate (5C) high-spin Fe^{III}-porphyrin thiolate model complex was determined to be 49%, which was reduced to 37% and 31% by one and two H-bonding interactions to the thiolate, respectively. Thus the 41 ± 3% covalency of the Fe-S bond in the substrate-bound high-spin P450 active site[34] indicates that it has one efficient H-bonding interaction to the thiolate, which is consistent with the published crystal structure.[33,35]

The XAS data for the resting low-spin ferric active site (Fig. 1, blue) shows an increase in pre-edge intensity relative to the substrate bound form (Fig. 1, red). The lack of resolvable transitions in the pre-edge indicates that the energy splitting between the t_2 and the e orbitals that covalently interact with the thiolate (i.e. S_{3p} mixed into these Fe wavefunction) is not large (a splitting of > 0.8 eV would be observed in the S K-edge spectrum). The total integrated intensity of these pre-edge transitions (Fig. 1) is 1.52 ± 0.03 centered at 2470.3 eV. This reflects the sum of the intensities of the transitions to the unoccupied t_2 and e holes ($t_2^5e_g^0$ ground configuration). This gives 56±2% S covalency, however note that according to the analyses of excited state multiplet effects for a S=1/2 Fe^{III} system presented in reference [36], only 75% of the intensity of the transitions to the e set contributes to the pre-edge energy region with the remaining 25% shifted to higher in energy (~ 1 eV, into the rising edge). This intensity can be estimated from the DFT calculations in section1B (25% of the S_{3p} in the e orbitals is 13%).[36] Thus the corrected total S_{3p} character in the Fe_{3d} manifold of the low-spin ferric resting active site is 69±2%. This increase in S_{3p} in the low-spin Fe^{III} resting form relative to the 41% S for the high spin Fe^{III} substrate bound form is expected as this bond is shorter in the low-spin form[2] (2.21 Å in low spin vs 2.36 Å in high-spin) and both the α and β Fe-S d-σ (i.e. e_g) orbitals are unoccupied in the low-spin complex relative to only the β component of each d-σ orbital in the high-spin complex. These results provide the key experimental parameters that were used to calibrate DFT calculations as described below.

B. DFT Calculations

i. Correlation to XAS data—Geometry optimizations for the low-spin ferric resting state were performed using an $FePSMeH_2O$ (where P = porphyrinato, SMe = thiolate) based model (Fig. 2A) and a larger model (Fig. 2B) where the backbone region of the Cys-Ile-Gly peptide sequence was also included (pdb id: 1DZ4).[33] The backbone N-H moiety of the Gly residue is within H-bonding distance of the S of the thiolate. The computational model of the active site was further expanded to include the H-bonding interactions from the Thr252 and Gly248 residues present in the distal pocket to the axial H_2O ligand (Fig. 2C). For the high-spin model (i.e. substrate bound) calculations, no axial H_2O ligand was included in the models A and B. The optimized structures using model A are in relatively good agreement with reported crystallographic data for both the high-spin substrate-bound[33,37] (Table 1, row 2) and crystallographic [38] and EXAFS data for the low-spin resting ferric state (Table 1, row 5).[3,39] In model A there is a noticeably large deviation of the optimized N-Fe-S-C torsion angle from that observed in crystallography. The heme plane has rotated along the Fe-S bond such that the optimized N-Fe-S-C torsion angle is 38° relative to 14° observed crystallographically. This

rotation is limited in the a-carbon constrained model B which is in better agreement with the crystallographic parameters (14° vs 17°).[35]

In general the calculated wavefunctions for all the high-spin 5C models (no H_2O bound) show that there are two bonding interactions between the thiolate S_{3p} donor orbitals and the iron Fe_{3d} orbitals; a d-σ interaction with the d_{z^2} orbital and a d-π interaction with the d_{yz} orbital (Fig. 3 for model B, Z-axis along the Fe-S bond, X-axis along the C-S bond). For model A, 26% S_{3p} is mixed into the d-π orbital and 21% S_{3p} is mixed into the d-σ orbital, giving 47% total S_{3p} character in the Fe_{3d} manifold, which is higher than the experimentally observed value of 41% (Table 1). Upon including the H-bonding interaction from the backbone to the thiolate in the model (model B), the d-π covalency decreases from 26% to 18% while the d-σ covalency remains unaffected. This is because the N-H of the peptide H-bonds only with the π donor S_{3p} orbital of the cysteine residue. A similar 8% decrease in Fe-S d-π covalency due to a single H-bond from an amide N-H was observed in the series of structurally characterized model complexes.[19] Thus H-bonding reduces the total Fe-S covalency to 40% in model B relative to 47% in the non H-bonded model A (experimental value is 41%, Table 1).

The wavefunction of the low-spin 6 co-ordinate (6C) model A-H_2O (i.e. resting, no substrate) has a total of 74% S_{3p} mixed into two Fe_{3d} orbitals; i.e. 22% S_{3p} is mixed into the β d-π and 52% S_{3p} is mixed into α and β d-σ orbital (Table 1). This is higher than the experimental observed value of 69%. Also note that the Fe-S σ bond covalency in the low-spin form is calculated to be higher than that of the high spin form (52% and 21% respectively) due to the presence of α and β unoccupied e orbitals in the $t_2^5e^0$ configuration of a low-spin Fe^{III} relative to only β unoccupied e orbitals in the $t_2^3e^2$ configuration of high-spin Fe^{III}. Inclusion of the H-bonding interaction to the thiolate ligand (model B-H_2O, Fig. 2B) decreases the $\%S_{3p}$ covalency to 69% (the d-π covalency reduced from 22% to 17% while the d-σ remains unaffected, Table 1). This is in agreement with the multiplet corrected experimental Fe-S covalency (69%, Table 1). Further expansion of the model to include the H-bonding interactions from the distal side to the axial H_2O ligand (CH_3OH representing the threonine residue, a non-coordinated H_2O molecule that H-bonds to the axial H_2O and an N-methylacetamide group representing the glycine group present in the distal pocket) leads to a slightly shorter Fe-O bond length in model C-H_2O (2.09 Å, Table 1, row 7) relative to model B-H_2O (2.15 Å, Table 1, row 6). This results in only a small decrease in Fe-S covalency to 67% in model C-H_2O relative to 69% in model B-H_2O.

In summary the experimental data and the computational results show that the Fe-S bond is very covalent in both the high-spin and low-spin states. The low-spin form is more covalent due to increased d-σ bonding interaction of the thiolate with low-spin Fe^{III}. Importantly, the H-bonding from the amide residue is directed towards the d-π S_{3p} orbital, which tunes down the π covalency in both the high-spin and low-spin models. Finally, it is important to note that the computational models with H-bonds to S (model B and C) agree well with the experimental results and can now be used to evaluate important reaction intermediates in the catalytic cycle.

ii. Reactivity

1. Reduction Potential: A key step in the catalytic cycle of P450 enzymes is reduction of the high-spin state, generated upon substrate binding, to the 5C ferrous form. The reduction potential of the 6C low-spin state is reported to be 125 mV more negative than of the corresponding high-spin site, which makes its reduction unfavorable.[4,40] The calculated ionization energies show that the low-spin active (ΔE_{6C}) site has 240 mV and 220 mV lower reduction potential than the high-spin active site (ΔE_{5C}) in the thiolate model A and the H-bonded thiolate model B, respectively, in general agreement with experimental value. To compare the reduction potentials of the different spin states, the reduction of the low-spin six co-ordinate Fe^{III} site (6C, S=1/2) to a five co-ordinate Fe^{II} site (5C, S=2) has been divided into

three steps: i) loss of an axial ligand (E_L in Scheme 1), ii) change of the spin state from S=1/2 to S=5/2 (E_{spin} in Scheme 1) and iii) reduction of the resultant 5C high-spin Fe^{III} site (5C, S=5/2) to a 5C Fe^{II} site (i.e. the functionally relevant potential, ΔE_{5C} in Scheme 1). We evaluate these contributions to the FeIII/II reduction potential of this heme thiolate active site below (i.e. 6C, S=1/2, $Fe^{III} + e^- \rightarrow$ 5C, S=2, Fe^{II}, $E_{6C} = E_L + E_{spin} + E_{5C}$, Scheme 1).

The energy decomposition in scheme 1 shows that this decrease in the reduction potential of the 6C site relative to the 5C site has two contributions both in the oxidized low-spin site ($\Delta E_L + \Delta E_{spin}$). Our calculations indicate that the axial H_2O ligand binding favors the 6C, S=1/2 FeIII state by 10 Kcal/mol (i.e. ΔE_L in Scheme 1 is −430 mV). Alternatively, the S=1/2 spin state is calculated to be disfavored relative to the S=5/2 spin state in the resultant Fe^{III} 5C site by 5 Kcal/mol (i.e. ΔE_{spin} in scheme 1 is calculated to be +220 mV). The net effect is that the binding energy of the water ligand in the ferric 6C S=1/2 state lowers the reduction potential by 220 mV relative to the 5C S=5/2 site.

We further investigated the contribution of the axial thiolate ligand in the redox properties of the substrate-bound high-spin 5C site (i.e. 5C, S=5/2, $Fe^{III} + e^- \rightarrow$ 5C, S=2, Fe^{II}, E_{5C} in Scheme 1) by comparing the calculated ionization energies (IE) of this site to those calculated with a neutral imidazole ligand and a fairly non-covalent anionic F^- ligand, and the tuning of the thiolate by H-bonding to the S (Table 2).[41] The calculated IE's in Table 2 with different axial ligands shows that relative to a neutral imidazole ligand, which is calculated to have an IE of 0.25 mV as a reference, the thiolate ligand shifts the $Fe^{III/II}$ potential more negatively by 1.38 V. This is in reasonable agreement with the > 1 V difference observed between the reduction potential of the thiolate bound heme (−680 mV) and imidazole bound heme (+350 mV) model complexes in the same non-coordinating solvent.[42,43] The non-covalent anionic ligand F^- (i.e. <10% F^- mixed in to the Fe_{3d} orbitals relative to > 40% for thiolate) is calculated to shift this $Fe^{III/II}$ potential negatively by 1.24 V relative to the neutral imidazole (Table 2). Thus, based on these calculated IE's the large negative shift in reduction potential associated with thiolate and F^- ligands may be interpreted as due to the additional stabilization of the oxidized Fe^{III} state by the anionic axial ligand. [11] However the electrostatic interaction between the Fe and thiolate is weaker than that between Fe and F^-. The Fe-S bond length in the thiolate complex (2.31 Å) is ~0.3 Å longer than that of the Fe-F bond (2.0 Å) resulting in a weaker electrostatic interaction and the negative charge on the thiolate is distributed over the anionic ligand. Also a significant amount of charge is donated from the thiolate to the Fe due to bonding. The IE for a P450 model with a hypothetical ionic thiolate ligand (modeled as a cluster of point charges using the NPAs of the thiolate bound to Fe) having the same geometry as the optimized structures, is calculated to be shifted by only −0.67 V relative to −1.24 V for F^-. Thus the contribution of the experimentally observed Fe-S covalency to the total ionization energy decrease of the thiolate complex is ~ −0.70 V, comparable to its electrostatic contribution.

The H-bonding to this axial thiolate ligand reduces the Fe-S bond covalency and tunes up the $Fe^{III/II}$ potential by +320 mV (Table 2, columns 3 and 4). A similar experimental shift in covalency and E° has been observed in the series of P450 model complexes and is due to stabilization of the electron density on the S in the reduced state.[19]

2. Compound 0: ***A. Geometric and electronic structure:*** Oxygen binding to Fe^{II} P450, further reduction and protonation lead to the formation of compound 0, a low-spin Fe^{III}-OOH species that is the last intermediate experimentally observed in the reaction cycle of P450.[44,45] In this section the experimentally calibrated low-spin thiolate bound Fe^{III}-OH_2 model developed above is extended to compound 0 by replacing the axial H_2O ligand by $^-$OOH. The effects of different structural perturbations of the axial thiolate and hydroperoxy ligands on the geometric and electronic properties of this hydroperoxy ferric species are evaluated and correlated to reactivity.

The optimized geometric parameters for the most stable conformations of the models A-OOH, B-OOH and C-OOH are listed in Table 3 and shown in Fig. 4 along with the calculated spin densities on relevant atoms. There are two limiting orientations for the low-spin heme thiolate hydroperoxide complex. In one conformation the C-S-O-O dihedral angle is close to 90° (Fig. 4B, anti) and in the other the C-S-O-O dihedral angle is close to 0° (Fig. 4B, syn). In models A-OOH and B-OOH the syn conformation is more stable than the anti by 5.5 Kcal/mol and 2.5 Kcal/mol, respectively (Table 3). The syn conformation has a shorter Fe-S distance and a higher spin density on the thiolate sulfur than the anti conformation which alternatively has a shorter Fe-O and higher spin density on O-O (Table 3, rows 1, 2 and 3, 4). This is because the singly occupied t_2 orbital on the low-spin Fe^{III} is delocalized over both the thiolate and the hydroperoxide ligand in the syn conformation whereas it is localized on the hydroperoxide ligand in the anti conformation (Fig. 5). This leads to a more covalent Fe-S d-π interaction in the syn conformation (reflected by the shorter Fe-S distance 2.40 in syn vs 2.45 Å in anti) which allows for additional energy stabilization and delocalization of the unpaired spin into the thiolate sulfur. Note that in case of model B the H-bonding to the thiolate sulfur weakens the d-π covalency (10% without H-bonding to 3% with H-bonding) which leads to a smaller energy difference between the two conformers (2.5 Kcal/mol) than in the non H-bonded model A-OOH (5.5 Kcal/mol).

Although no structural parameters for compound 0 have been reported for comparison, the C-S-O-O dihedral angle may be inferred from the crystal structure of the dioxygen-bound ferrous active site, which is ~40°. This orientation of the Fe-O-O plane is important as it enables the distal oxygen to H-bond to the conserved threonine residue, which is the proposed proton source for the generation of compound 0 as well as the proton for O-O bond cleavage.[46] Inclusion of the proximal H-bonding to cysteine S atom and distal H-bonding interactions from threonine (modeled by CH_3OH), H_2O and a glycine (modeled by acetamide) in the computational model C-OOH reproduces this C-S-O-O dihedral angle (47.8° calculated vs 40° experimental) as well as the H-bonding interaction between the distal oxygen of the OOH and the threonine O-H. As noted earlier the syn conformer is expected to be more stable by 5.5 Kcals/mol due to more favorable bonding interactions. However the H-bonding interaction to the cysteine lowers this energy difference to 2.5 Kcals/mol and the additional H-bonding of the hydroperoxy with the distal CH_3OH residue further stabilizes this orientation. This H-bonding from the distal pocket results in a weaker Fe-OOH bond in model C-OOH relative to model B-OOH in the more stable syn conformation, which is reflected in the longer Fe-O bond length and decreased spin density on the peroxide fragment in model C-OOH (Table 3, row 5). This weakening of the Fe-O bond in model C-OOH is reciprocated by strengthening of the trans Fe-S interaction, as indicated by a shorter (2.37 Å) Fe-S bond and an increased spin density (0.05) on the sulfur atom relative to the more stable syn B-OOH model (Fe-S 2.45 Å, spin 0.0).

B. Reactivity: Compound 0 can decay via i) protonation and heterolytic O-O bond cleavage leading to the formation of compound I (the generally considered reaction), ii) protonation and heterolytic cleavage of the Fe-O bond leading to H_2O_2 release (i.e. uncoupled reaction), iii) homolytic O-O bond cleavage (proposed for certain mutants), and iv) direct H-atom abstraction (Scheme 2). In this section the calculated energies (ΔE) for these processes for the H-bonded thiolate ligand (model B) are compared to those for a neutral imidazole and the fairly non-covalent anionic F^- ligand (the optimized geometries of relevant species are listed in Table 4, their Mulliken spin densities are listed in Table 5 and the calculated energies are listed in Table 6). The ΔE for protonation assisted heterolytic O-O bond cleavage generating a compound I species and a H_2O molecule is about −46 Kcal/mol for a trans thiolate ligand with H-bonding (model B). The ΔE for a neutral imidazole ligand is only −20 Kcal/mol. A calculation with an axial anionic F^- ligand gives a ΔE for compound I formation of −40 Kcal/mol, which is −20 Kcal/mol more negative than the reference neutral imidazole ligand.[47] This indicates that the

covalent anionic axial thiolate ligand greatly favors the formation of compound I relative to a neutral axial ligand (i.e. imidazole) consistent with previous results.[11] Note that this difference in ΔE's of compound I formation between an imidazole and a thiolate axial ligand is generally referred to as the "push" effect of the thiolate ligand in cytochrome P450.[48] The more favorable ΔE could reflect an increased proton affinity of the compound 0 species or an additional stabilization of the resulting compound I species by the axial thiolate ligand. These factors are evaluated below.

The protonation of the distal oxygen of compound 0 leads to spontaneous formation and dissociation of a water molecule and formation of compound I during geometry optimization which complicates estimation of its proton affinity.[49] However, protonation of the proximal oxygen leads to the formation of a stable Fe^{III}-O_2H_2 species and can be used to obtain an estimate of the proton affinity of compound 0. The proton affinity of compound 0 with a thiolate ligand is −33 Kcal/mol, which is 4 Kcal/mol more negative than that for an anionic F^- ligand (−29 Kcal/mol). On the other hand, for a neutral axial ligand such as imidazole the proton affinity is only −9 Kcal/mol. Therefore, the thiolate ligand increases the proton affinity of compound 0 relative to the neutral ligand by 24 Kcal/mol. Thus, out of the 26 Kcal/mol difference in ΔE for the formation of compound I from compound 0 with an axial thiolate relative to a neutral imidazole ligand, 24 Kcal/mol is derived from its greater proton affinity and only 2 Kcal/mol results from additional stabilization of the resultant compound I species by the axial thiolate ligand.

The large negative proton affinity of the proximal oxygen indicates that formation of an $Fe^{III}O_2H_2$ species is energetically favorable in the P450 active site (Scheme 2, proton from solvent is worth 262 Kcal/mol).[50] Cleavage of the Fe-O bond in this $Fe^{III}O_2H_2$ species forming a high-spin 5C site with release of H_2O_2 is estimated to be +10 Kcal/mol uphill in energy (Scheme 2).[51] It is important to note that while this is uphill, the protonation of the proximal oxygen of compound 0 forming the Fe^{III}-O_2H_2 is energetically favorable (−33 Kcal/mol). Thus the orientation of the Fe-O-O plane in compound 0 in the optimized structure (model C-OOH, Fig. 4) is an important contribution to its reactivity, as it directs the protonation to the distal oxygen, initiating the heterolytic O-O bond cleavage while minimizing the possibility of H_2O_2 formation via a protonation on the proximal oxygen of compound 0.[2] The threonine 252 residue which is H-bonded to the distal oxygen of compound 0 (model C) ensures that this oxygen gets protonated, leading to heterolytic O-O bond cleavage and formation of compound I. In the absence of this residue there can be loss of selectivity in protonation of compound 0, which would also lead to H_2O_2 formation via an uncoupling reaction.[9]

The calculations indicate that ΔE for O-O bond homolysis is +24-28 Kcal/mol uphill (Table 6) for all the axial ligands tested, suggesting that this pathway is unfavorable relative to either of the two proton assisted pathways considered above. The ΔE for O-O bond homolysis shows only a minor dependence on the nature of the axial ligand.[52] Newcomb *et al.* have proposed that compound 0 reacts directly with the substrate, possibly via H-atom abstraction,[53] a reaction similar to that of activated bleomycin.[54] The H-atom abstraction energy for an alkyl C-H bond (the bond strength used here is 101 Kcal/mol) is calculated to be endothermic by +4-6 Kcal/mol (Table 6). The calculated H-atom abstraction energies are independent of the nature of the axial ligand, which is consistent with the invariance seen in the calculated energies for O-O bond homolysis. Note that while the ΔE for H-atom abstraction by compound 0 is calculated here to have a ΔE of +4-6 Kcal/mol, this process has been calculated by Shaik *et. al.* to have a barrier of ~17 Kcal/mol ($G^{\ddagger}$).[55,2]

3. Compound I and Compound II: Compound I has been described as a $P^{-\cdot}$Fe(IV)=O species, where $P^{-\cdot}$ represents a porphyrin monoanion radical species. It is generally accepted that this species performs an H-atom abstraction from a substrate forming compound II, which is either

an Fe(IV)-OH species (with axial thiolate ligand; P450) or Fe^{IV}-O species (with an axial imidazole ligand; peroxidases).[56,57] For a parallel comparison of the different axial ligands we have focused on the former species. The strength of the C-H bond that can be abstracted by compound I with different axial ligands (i.e. the O-H bond strength of the resulting compound II species) will depend on both the reduction potential of compound I and the proton affinity of the resultant Fe(IV)=O species.[58] A more positive reduction potential and higher proton affinity will increase the BE_{O-H} (B.E. = bond energy). Table 7 lists the calculated O-H bond energies of the compound II species, their ionization energies without a proton and proton affinities for axial imidazole and fluoride ligands relative to those for a thiolate ligand. The calculated BE_{O-H} is −96 Kcal/mol for a thiolate axial ligand, which is reasonable based on the known bond energies of aliphatic C-H bonds abstracted by compound I. Interestingly, the relative ΔBE_{O-H} is only 4.0 Kcal/mol higher with an axial imidazole ligand relative to a thiolate. This is because the two contributions to BE_{O-H} vary differently with the nature of axial ligand. From Table 7 and Scheme 3 the anionic thiolate ligand increases the proton affinity of the Fe (IV)=O species. Thus the E_{proton} term is 32.5 Kcal/mol more favorable for a thiolate ligand relative to a neutral imidazole ligand. However, the anionic nature of the thiolate also lowers the ionization energy of compound II. This disfavors the BE_{O-H} by 28.5 Kcal/mol relative to a neutral imidazole ligand. Together these result in very similar ΔBE_{O-H} for compound I sites with both neutral and anionic axial ligands.

Geometry optimizations indicate that similar to compound 0, compound II also has two possible orientations of the Fe-OH plane relative to the C-S-Fe plane: syn, when the C-S-O-H dihedral angle is 0° and anti, when the angle is 90° (Scheme 4). The orientation of the camphor C-H bond relative to the Fe-S-C plane in the crystal structure of the Fe-O_2 form suggests that the Fe(IV)-OH species that would result immediately after the first H-atom abstraction step could be in the anti conformation (Scheme 4).[59] The Fe-O-H plane of this species has to rotate 90° to form the syn conformer for the rebound hydroxylation step to take place. This energy difference between the syn and the anti conformations is the reorientation energy invoked by Shaik *et al.* and Yoshizawa and coauthors, which is estimated to be 1–8 Kcal/mol depending on the method used.[60–63] The DFT calculations for model A without the H-bond to the thiolate indicate that, in contrast to compound 0, where the syn conformation was more stable, the anti conformation of compound II is more stable by 1.5 Kcal/mol. This is because in an S=1 Fe(IV) system, two d-π holes are available for π bonding with both the thiolate and hydroxide ligands which have one π donor valence orbital each (Fig. 7, top). In the anti conformation both the thiolate and the hydroxide ligand can form strong orthogonal π donor bonds. However, in the syn conformation, these ligands compete to form π donor bonds to the same d-π orbital. This is indicated by longer Fe-O and FeS bond lengths and reduced spin densities on both the thiolate and hydroxide ligands in the syn conformation relative to the anti conformation (Table 8). The reorientation for rebound thus involves a barrier as the final syn conformer is at higher energy than the initial anti conformer. H-bonding to the thiolate (model B) weakens the Fe-S d-π bond and reduces this ΔE to only 0.8 Kcal/mol at this level of calculation.[64]

The rotation of the O-H bond to a syn conformation leads to an FMO (Fig. 7, bottom) that is set-up for hydroxyl transfer to the carbon radical on the substrate. The energy of this step ($\Delta E_{CompII-Fe(III)}$, Table 8) reflects the homolytic dissociation energy of the Fe^{IV}-OH bond in compound II. The lower 6 Kcal/mol Fe^{IV}-OH homolytic bond dissociation of compound II with a thiolate axial ligand relative to imidazole reflects its stronger trans effect weakening the Fe-OH bond.

Discussion

The S K-edge XAS results provide insight into the role of the axial thiolate ligand in the active site of cytochrome P450. The thiolate ligand is a very covalent anionic ligand. Our experimental

data indicate that in the resting high-spin state of P450cam the covalency of this bond is 41% (i.e. 0.41 S_{3p} character of the thiolate is mixed into the d orbitals of the Fe^{III}) and it is 69% (corrected for multiple effects) in the resting low-spin state. Correlation to previously published data on structurally characterized model complexes indicates that this electronic structure reflects one strong H-bond to the cysteine sulfur in the P450cam active site[19] consistent with crystallography and biochemical studies.[12,33] Consistent with the experiment, the DFT calculations indicate that binding of an additional H_2O axial ligand in the low-spin form lowers its reduction potential by ~230 mV relative to the high-spin 5C active site. This reflects the opposite effects of ligand binding and spin state of the oxidized state. These calculations further show that the axial thiolate ligand lowers the $Fe^{III/II}$ reduction potential by ~ 1 V relative to a neutral imidazole ligand as observed in models.[42,43] This is reflects the strong bonding of the axial thiolate ligand with the oxidized Fe center. Half derives from the anionic nature of the thiolate and half results from very covalent Fe-S interaction observed experimentally. The calculations further indicate that the experimentally observed H-bonding effect on the Fe-S bond tunes this potential up by +320 mV.[65]

The push-effect of the axial thiolate ligand has been proposed to weaken the O-O bond, activating it for heterolytic cleavage. Our calculations with imidazole and thiolate axial ligands indicate that the axial thiolate does not weaken the O-O bond in compound 0 relative to a neutral imidazole ligand (same O-O bond distance and O-O homolysis energy). Instead the anionic nature of the thiolate raises the pKa of compound 0, favoring its protonation by ~20 Kcal/mol relative to a neutral imidazole ligand. Thus the inherently high pKa of the thiolate bound heme active site activates it to undergo proton induced heterolytic cleavage of the O-O bond. Note that this energy decomposition scheme is different from that presented by Shaik and co-workers[11] where O-O bond homolysis is followed by the oxidation of the resultant ferryl by the generated hydroxyl radical and the ^{-}OH produced is then protonated. The role of the thiolate ligand was found to lower the reduction potential of the ferryl species.[11] However the idea that the charge of the thiolate is playing a dominant role in the O-O heterolysis is consistent with the fact that a proton is required for the formation of compound I. Also calculations where the thiolate is replaced by a poor donor F^{-} indicate that the electrostatic effect of an anionic ligand is as efficient as a covalent thiolate in driving the proton assisted formation of compound I from compound 0. Thus the push effect of a thiolate is similar to that of an anionic ligand which c raises the pKa of compound 0 and drives the proton assisted O-O bond heterolysis.

It has been proposed that the strong proton affinity of this thiolate bound Fe^{IV}=O species provides the large driving force for H-atom abstraction by compound I.[56,57] The computational results presented here indicate that, while the thiolate provides a large driving force for protonation, the nature of the axial ligand has only a very limited effect on the overall energy of H-atom abstraction by compound I (i.e. $BE_{O\text{-}H}$, Table 7). This is because the nature of the axial ligand has opposing effects on the contributions to H-atom abstraction (IE and pKa). As discussed by Green and coworkers, compound I with an anionic thiolate ligand has a lower IE, however the resulting Fe^{IV}=O species has a higher proton affinity.[57] Alternatively, a neutral axial ligand like imidazole has a lower proton affinity of the Fe^{IV}=O, but the higher IE of this species leads to a comparable driving force for H-atom abstraction. However a 4 Kcal/mol difference in ΔE (i.e. imidazole vs thiolate axial ligand in Table 7) can still lead to as much as ~ 10^3 times lower rate. In fact, Nam *et al.* has found that a compound I species with a neutral axial ligand is capable of C-H bond hydroxylation although its rate is 650 times slower than the rate observed for an anionic axial ligand.[66] Also when the axial cysteine ligand is mutated to histidine in P450 it still shows some camphor hydroxylation.[67] Interestingly this mutant also shows a significant increase (100 fold) in peroxidase activity (oxidation of guaiacol using H_2O_2 as oxidant).[67] Thus although a compound I species with an axial imidazole ligand is capable of C-H bond hydroxylation, its high reduction potential increases its effectiveness for

outer sphere oxidation. The presence of an anionic thiolate ligand increases the selectivity for C-H bond hydroxylation relative to outer sphere oxidation by lowering the potential and raising the pKa of compound I.

Thiolate is a strong anisotropic π donor that can restrict the rotation of anisotropic π donor trans-axial ligands in particular $^{-}$OH and $^{-}$OOH about their Fe-O axis. In the case of compound 0, the most stable geometry requires the thiolate and hydroperoxide ligands be in the syn conformation, where they are both able to π donate into the only available singly occupied t_2 orbital on the S = 1/2 Fe^{III} center. However, for compound 0 to H-bond to tyrosine 252 the Fe-O-OH plane needs to rotate 48°, from its most energetically stable geometry.[1,33] This rotation is calculated to have a barrier of 5.5 Kcal/mol for compound 0. This may compromise catalytic efficiency as H/D isotope data and cryoreduction experiments [46,68] and recent QM/MM calculations[69,70] indicate that the protonation of compound 0 may be the rate determining step in substrate oxidation. However, the presence of a strong H-bonding interaction with the thiolate, reflected in the pre-edge intensity of the S K-edge XAS data in Fig. 1, tunes this anisotropic π covalency down, which significantly lowers this rotational barrier and facilitates reorientation of the trans hydroperoxide ligand to a conformation that would enhance reactivity. Alternatively, in compound II, the thiolate and hydroxide ligands need to be in an anti orientation to individually form π bonds with the two orthogonal singly occupied t_2 orbitals on the S=1 Fe^{IV} center. For rebound, this OH bond has to rotate 90° off this alignment which is slightly endothermic by 1.5 Kcal/mol. This barrier is also lowered by the H-bonding to the thiolate.

In summary, S K-edge XAS data on cytochrome P450 provide key experimental Fe-S bond covalencies for this active site. The thiolate is a very covalent anionic ligand that: 1) lowers the reduction potential of the active site, and 2) raises the pKa of the Fe^{III}-OOH, compound 0, leading to its protonation that drives O-O bond heterolysis. There is one strong H-bond to the thiolate S of the active site that: 1) tunes the potential by > 200mV, and 2) eliminates the anisotropic π covalency which lowers rotational barriers of bound oxygen intermediates facilitating proton transfer and rebound.

Supplementary Material

Refer to Web version on PubMed Central for supplementary material.

Acknowledgments

This research was supported by NIH Grants 0446304 (E.I.S.), RR-01209 (K.O.H.), GM25515 (P.O.M.). SSRL operations are supported by the Department of Energy, Office of Basic Energy Sciences. The SSRL Structural Molecular Biology Program is supported by the National Institutes of Health, National Center for Research Resources, Biomedical Technology Program, and by the Department of Energy, Office of Biological and Environmental Research. Dr. Takehiro Otah is acknowledged for helpful discussions. This publication was partly made possible by Grant Number 5 P41 RR001209 from the National Center for Research Resources (NCRR), a component of the National Institutes of Health (NIH). Its contents are solely the responsibility of the authors and do not necessarily represent the official view of NCRR or NIH.

References

1. Denisov IG, Makris TM, Sligar SG, Schlichting I. Chem Rev 2005;105:2253–2278. [PubMed: 15941214]
2. Shaik S, Kumar D, deVisser SP, Altun A, Thiel W. Chem Rev 2005;105:2279–2328. [PubMed: 15941215]
3. Hahn JE, Hodgson KO, Andersson LA, Dawson JH. J Biol Chem 1982;257:10934–10941. [PubMed: 7107639]
4. Sligar SG. Biochemistry 1976;15:5399–5406. [PubMed: 187215]

5. Raag R, Poulos TL. Biochemistry 1989;28:917–922. [PubMed: 2713354]
6. Loew GH, Harris DL. 2000;100:407–420.
7. Sono M, Roach MP, Coulter ED, Dawson JH. Chem Rev 1996;96:2841–2887. [PubMed: 11848843]
8. Raag R, Martinis SA, Sligar SG, Poulos TL. 1991;30:11420–11429.
9. Martinis SA, Atkins WM, Stayton PS, Sligar SG. J Am Chem Soc 1989;111:9252–9253.
10. Deng T, Proniewicz LM, Kincaid JR, Yeom H, Macdonald IDG, Sligar SG. Biochemistry 1999;38:13699–13706. [PubMed: 10521277]
11. Ogliaro F, de Visser SP, Shaik S. J Inorg Biochem 2002;91:554–567. [PubMed: 12237222]
12. Deng, Tj; Macdonald, IDG.; Simianu, MC.; Sykora, M.; Kincaid, JR.; Sligar, SG. J Am Chem Soc 2001;123:269–278. [PubMed: 11456513]
13. Glaser T, Hedman B, Hodgson KO, Solomon EI. Acc Chem Res 2000;33:859–868. [PubMed: 11123885]
14. Solomon EI, Hedman B, Hodgson KO, Dey A, Szilagyi RK. Coord Chem Rev 2005;249:97–129.
15. Neese F, Hedman B, Hodgson KO, Solomon EI. Inorg Chem 1999;38:4854–4860. [PubMed: 11671216]
16. Glaser T, Bertini I, Moura JJG, Hedman B, Hodgson KO, Solomon EI. J Am Chem Soc 2001;123:4859–4860. [PubMed: 11457306]
17. Dey A, Glaser T, Moura JJG, Holm RH, Hedman B, Hodgson KO, Solomon EI. J Am Chem Soc 2004;126:16868–16878. [PubMed: 15612726]
18. Rose K, Shadle SE, Glaser T, de Vries S, Cherepanov A, Canters GW, Hedman B, Hodgson KO, Solomon EI. J Am Chem Soc 1999;121:2353–2363.
19. Dey A, Okamura T, Ueyama N, Hedman B, Hodgson KO, Solomon EI. J Am Chem Soc 2005;127:12046–12053. [PubMed: 16117545]
20. De Voss JJ, Sibbesen O, Zhang Z, Ortiz de Montellano PR. J Am Chem Soc 1997;119:5489–5498.
21. Hedman B, Frank P, Gheller SF, Roe AL, Newton WE, Hodgson KO. J Am Chem Soc 1988;110:3798–3805.
22. George, GN. EXAFSPAK & EDG_FIT; Stanford Synchrotron Radiation Laboratory, Stanford Linear Accelerator Center. Stanford University; Stanford, CA: 2000.
23. Agarwal B. XRAY SPECTROSCOPY 1979:276.
24. Tyson TA, Roe AL, Frank P, Hodgson KO, Hedman B. Phys Rev B 1989;39:6305–6315.
25. Frisch, MJT., et al. Gaussian 03. Vol. C02. Gaussian, Inc; Wallingford CT: 2004.
26. Becke AD. Phys Rev A 1988;38:3098–3100. [PubMed: 9900728]
27. Perdew JP. Phys Rev B Condensed Matter 1986;33:8822–8824.
28. Becke AD. Journal of Chemical Physics 1993;98:5648–5652.
29. Lee C, Yang W, Parr RG. Phys Rev B Condensed Matter 1988;37:785.
30. Miertus S, Scrocco E, Tomasi J. Chem Phys 1981;55:117–129.
31. Mulliken RS. J of Chem Phys 1955;23:1833–1840.
32. Tenderholt, AL. PyMOlyze, Version 1.1. http://pymolyze.sourceforge.net
33. Schlichting I, Berendzen J, Chu K, Stock AM, Maves SA, Benson DE, Sweet RM, Ringe D, Petsko GA, Sligar SG. Science 2000;287:1615–1622. [PubMed: 10698731]
34. It has been shown that there is no 6th ligand in the high-spin state.
35. Poulos TL, Finzel BC, Howard AJ. J Mol Biol 1987;195:687–700. [PubMed: 3656428]
36. Dey A, Jenney FE, Adams MWW, Johnson MK, Hodgson KO, Hedman B, Solomon EI. J Am Chem Soc 2007;129:12418–12431. [PubMed: 17887751]
37. Schlichting I, Jung C, Schulze H. FEBS Lett 1997;415:253–257. [PubMed: 9357977]
38. Poulos TL, Finzel BC, Howard AJ. Biochemistry 1986;25:5314–5322. [PubMed: 3768350]
39. Cramer SP, Dawson JH, Hodgson KO, Hagerlc LP. J Am Chem Soc 1978;100:7282–7290.
40. Backes WL, Tamburini PP, Jansson I, Gibson GG, Sligar SG, Schenkman JB. Biochemistry 1985;24:5130–5136. [PubMed: 3935158]
41. Note that the model B and C has very similar electronic structure. Hence we use model B to evaluate ionization energy shifts as it is more computationally economic.

42. Ueyama N, Nishikawa N, Yamada Y, Okamura T, Oka S, Sakurai H, Nakamura A. Inorg Chem 1998;37:2415–2421.
43. Collman JP, Boulatov R, Sunderland CJ, Fu L. Chem Rev 2004;104:561–88. [PubMed: 14871135]
44. Davydov R, Macdonald IDG, Makris TM, Sligar SG, Hoffman BM. J Am Chem Soc 1999;121:10654–10655.
45. Mak PJ, Denisov IG, Victoria D, Makris TM, Deng T, Sligar SG, Kincaid JR. J Am Chem Soc 2007;129:6382–6383. [PubMed: 17461587]
46. Yano JK, Blasco F, Li H, Schmid RD, Henne A, Poulos TJ. J Biol Chem 2003;278:608. [PubMed: 12401810]
47. As shown in section ii, 1 the charge on a thiolate bound to iron is less and the distance from Fe is larger than an anionic ligand like F-.
48. Dawson JH. Science 1988;240:433–439. [PubMed: 3358128]
49. Harris DL, Loew GH. J Am Chem Soc 1998;120:8941–8948.
50. Noyes RM. J Am Chem Soc 1962;84:513–522.
51. However this reaction involves a barrier associated with the forbidden two-electron spin flip.
52. The imidazole axial ligand has ~ 4 Kcal/mol lower ΔE for hemolytic cleavage relative to a F- or a thiolate ligand. This can be attributed to the stronger Fe-O bonding in the product ferryl species (1.62Å, Table 4) due to its relatively weak trans effect compared to a thiolate ligand (Fe-O 1.65Å, Table 4). The stronger Fe-O bond in the resultant ferryl species is also indicated by the higher spin density on the oxygen of the ferryl unit (which reflects the covalency of the Fe-O bond) when imidazole ligand is trans to it. However it must be emphasized that the calculations reflect lack of any significant effect of the axial ligand on the ΔE of the hemolytic O-O cleavage of compound 0.
53. Chandrasena REP, Vatsis KP, Coon MJ, Hollenberg PF, Newcomb M. J Am Chem Soc 2004;126:115–126. [PubMed: 14709076]
54. Decker A, Chow MS, Kemsley JN, Lehnert N, Solomon EI. J Am Chem Soc 2006;128:4719. [PubMed: 16594709]
55. Derat E, Kumar D, Hirao H, Shaik S. J Am Chem Soc 2006;128:473–484. [PubMed: 16402834]
56. Green MT, Dawson JH, Gray HB. Science 2004;304:1653–1656. [PubMed: 15192224]
57. Behan RK, Hoffart LM, Stone KL, Krebs C, Green MT. J Am Chem Soc 2006;128:11471–11474. [PubMed: 16939270]
58. Gardner KA, Kuehnert LL, Mayer JM. Inorg Chem (Washington, DC, U S) 1997;36:2069–2078.
59. Note that this orientation is unlikely to change during the formation of compound 0 as both the Camphor and the Cysteine thiol is held tightly in their orientation in the protein active site.
60. Shaik S, Cohen S, de Visser SP, Sharma PK, Kumar D, Kozuch S, Ogliaro F, Danovich D. Eur J Inorg Chem 2004:207–226.
61. Kamachi T, Yoshizawa K. J Am Chem Soc 2003;125:4652–4661. [PubMed: 12683838]
62. Hata M, Hirano Y, Hoshino T, Tsuda M. J Am Chem Soc 2001;123:6410–6416. [PubMed: 11427068]
63. Kamachi T, Yoshizawa K. J Am Chem Soc 2003;125:4652–4661. [PubMed: 12683838]
64. Note that the relative to other anionic trans-axial ligands like F-, the FeIV-OH bond is longer in the thiolate coordinated model. This is because of the strong σ covalency of a thiolate ligand that weakens the trans axial Fe-OH bond.
65. Fisher MT, Sligar SG. J Am Chem Soc 1985;107:5018–5019.
66. Song WJ, Ryu YO, Song R, Nam W. J Biol Inorg Chem 2005;10:294–304. [PubMed: 15827730]
67. Auclair K, Moenne-Loccoz P, Ortiz de Montellano P. J Am Chem Soc 2001;123:4877–4885. [PubMed: 11457314]
68. Davydov R, Makris TM, Kofman V, Werst DE, Sligar SG, Hoffman BM. J Am Chem Soc 2001;123:1403–1415. [PubMed: 11456714]
69. Zheng J, Wang D, Thiel W, Shaik S. J Am Chem Soc 2006;128:13204–13215. [PubMed: 17017800]
70. Chen H, Hirao H, Derat E, Schlichting I, Shaik S. J Am Chem Soc 2008;112:9490–9500.

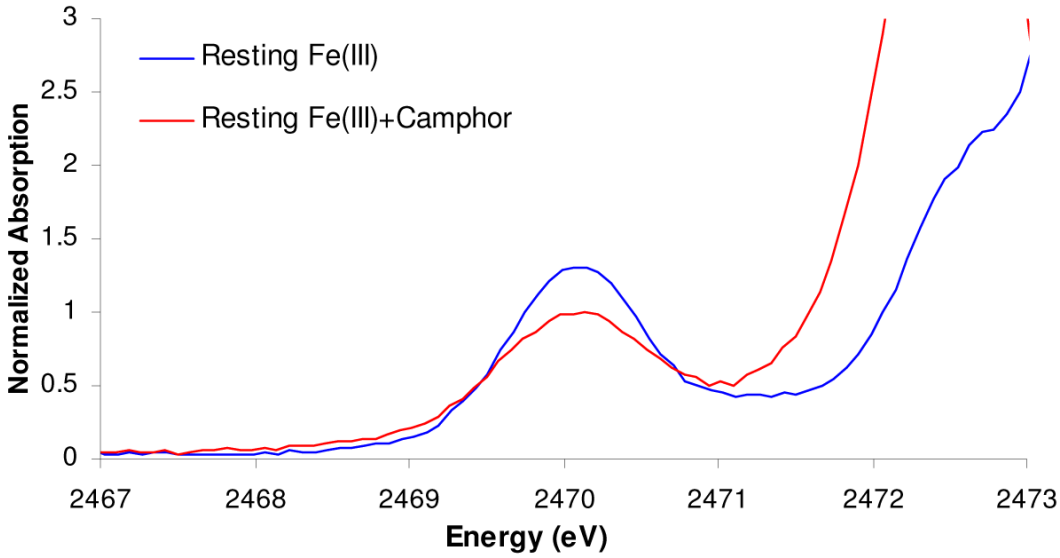

Figure 1.
Background subtracted S K-edge XAS data of resting ferric (blue) and camphor bound ferric (red) cytochrome P450.

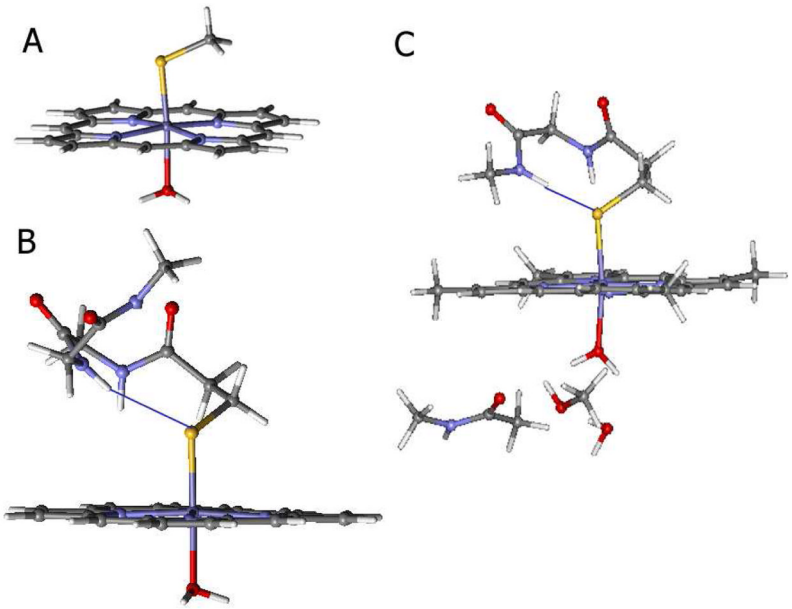

Figure 2.

Structural models for the calculations of the resting ferric site used in this study. A) Porphyrin ligand with water and thiolate axial ligands; B) An expanded to include H-bonding from the backbone to the thiolate (indicated by a blue line); and C) B expanded to include H-bonding to the ligand in the distal pocket. For the substrate-bound site, the H_2O was eliminated and models A and B applied.

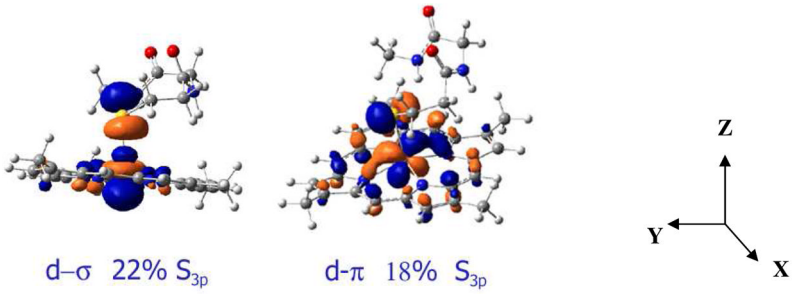

Figure 3.
The d-σ (left) and d-π (right) interaction between a thiolate ligand and a 5C high-spin Fe^{III} (model B). The reference co-ordinate system is shown.

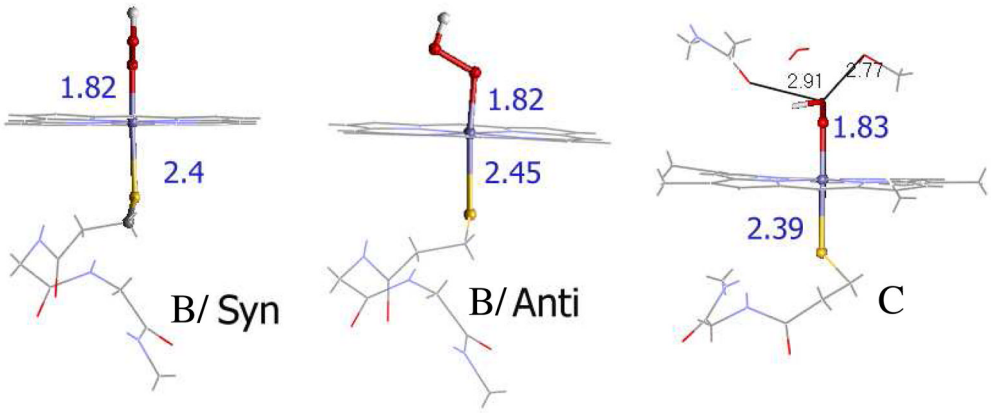

Figure 4.

Optimized geometries of compound 0 model B (two left structures). In the syn orientation, the O-O bond projects into the plane of the paper whereas it is in the plane in the anti orientation. The structure on the right is the optimized model C with the $^{-}$OOH ligand. Fe-S, Fe-O and H-bonding distances with the distal hydroperoxide ligand are indicated. (Iron in blue, sulfur in yellow, oxygen in red.)

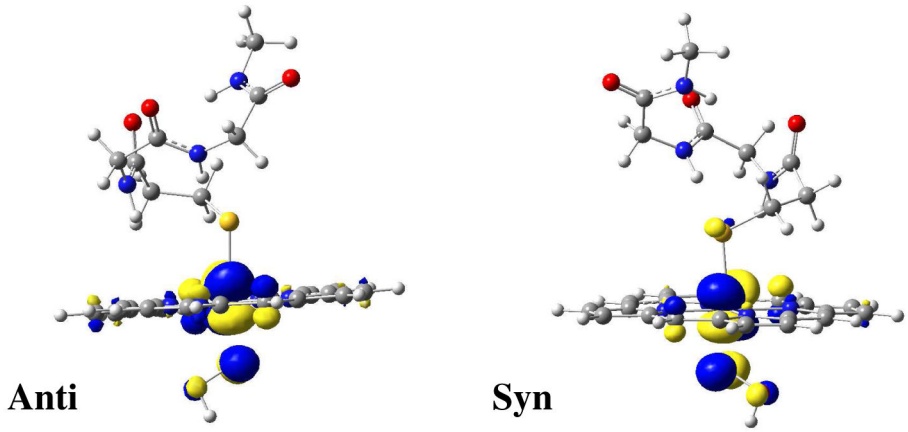

Figure 5.
Representative t_2 SOMO's of the anti (left) and syn (right) conformations using Model B-OOH (OOH ligand is in the plane of paper). Contributions from individual donor ligands are given in Table 3.

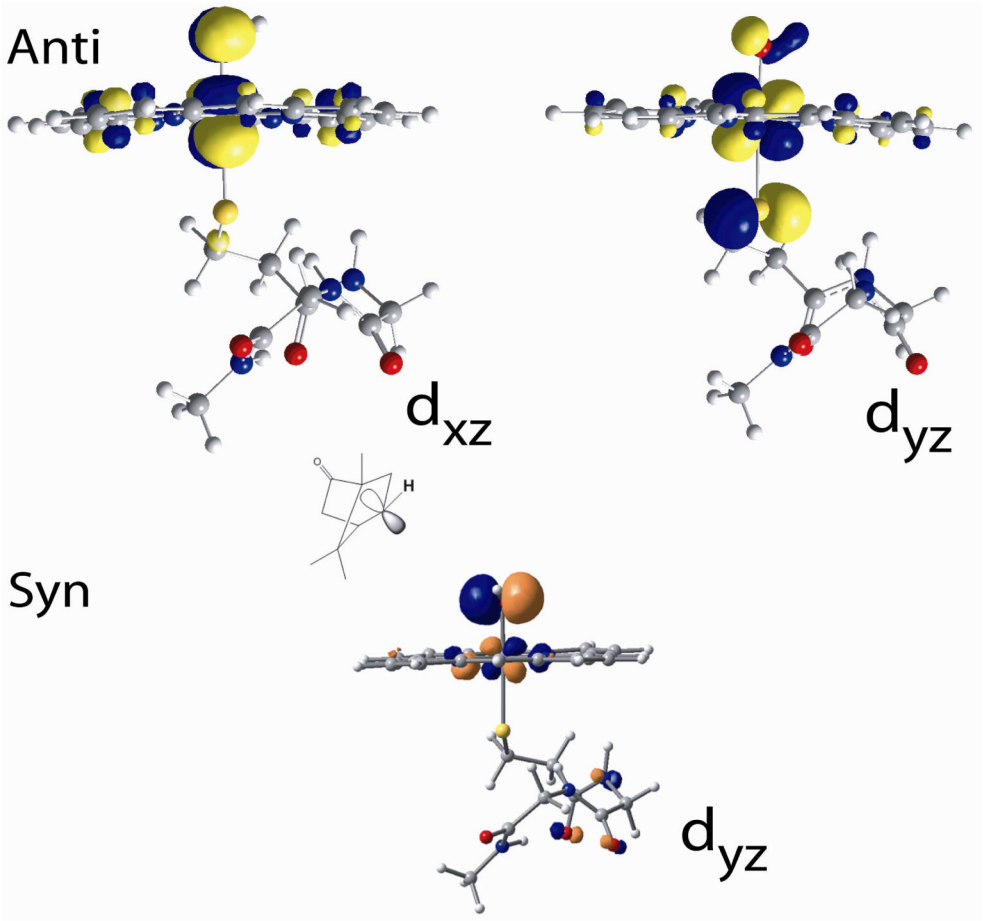

Figure 7.
The β Fe^{IV}-OH d-π SOMOs in the anti (top) and syn (bottom) configuration of model B. In the latter case the oxygen donor orbital is directed towards the C-OH bond (carbon acceptor orbital indicated for clarity) to be formed.

$$Fe^{III}\text{-}OH_2\,(6C,\ S=1/2) \rightarrow Fe^{III}\,(5C,\ S=1/2) + H_2O \qquad \Delta E_L$$

$$Fe^{III}\,(5C,\ S=1/2) \rightarrow \quad Fe^{III}\,(5C,\ S=5/2) \qquad \Delta E_{spin}$$

$$Fe^{III}\,(5C,\ S=5/2) + e^- \rightarrow Fe^{II}\,(5C,\ S=2) \qquad \Delta E_{5C}$$

Scheme 1.
Steps in the reduction of the 6C, S=1/2 resting Fe^{III} state

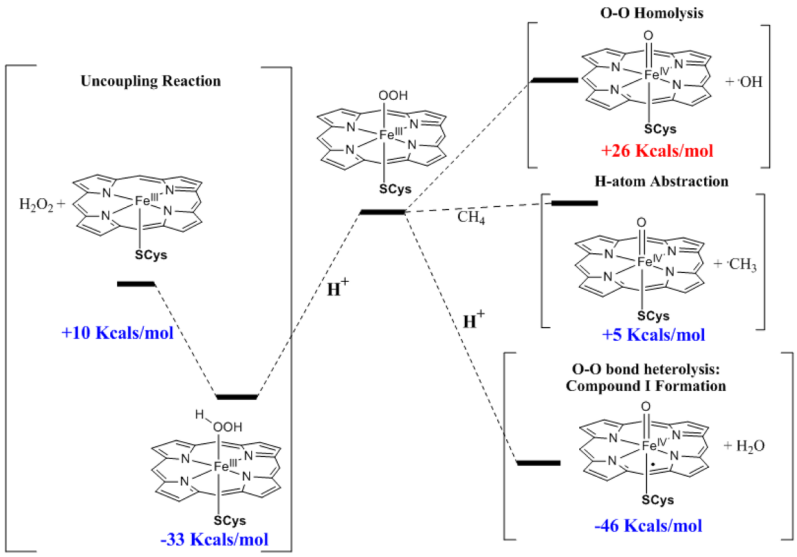

Scheme 2.
Three different reactions of compound 0.

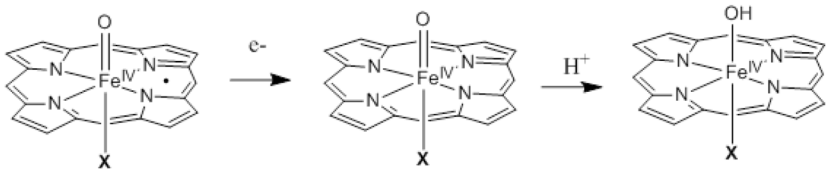

Scheme 3.
The two contributions to H-atom abstraction by compound I.

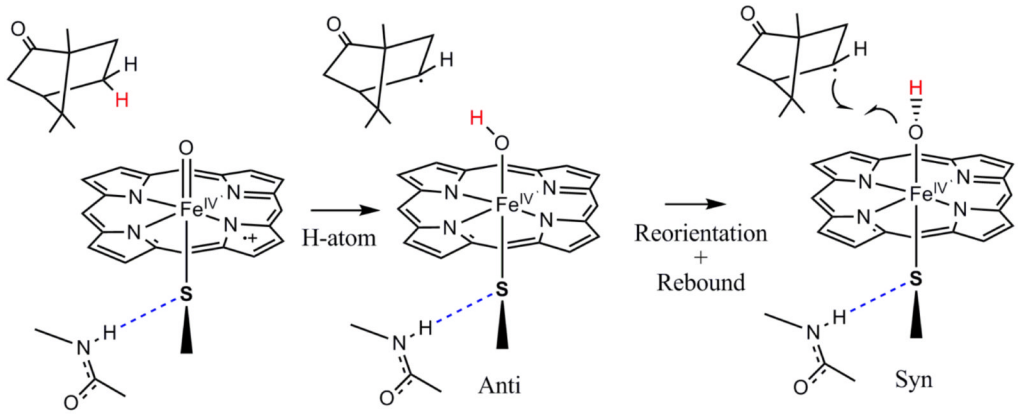

Scheme 4.
Involvement of an anti to syn reorientation of compound II during rebound.

Table 1

Geometric Parameters and Fe-S Covalencies of Computational Models A, B, C and the Experimental Values (in Bold).

		Distances (Å)				Angles (°)[a]		%S_{3p}		
		Fe-S	***Fe-N***	***Fe-L_{axial}***	***N- - - S***	***Fe-S-C***	***N-Fe-S-C***	***π***	***Σ***	***Total***
Substrate Bound		***2.36***	***2.05***			***108–112***	***7–17***			***41±2***
A	*S=5/2*	*2.31*	*2.09*			*106*	*38*	*26*	*21*	*47*
B	*S=5/2*	*2.32*	*2.08*		*3.41*	*112*	*14*	*18*	*22*	*40*
Resting Ferric		***2.22***	***2.00***	***2.0***		***106***	***11***			***69±2***
A+H_2O	*S=1/2*	*2.21*	*2.01*	*2.17*		*112*	*47*	*22*	*52*	*74*
B+H_2O	*S=1/2*	*2.22*	*2.01*	*2.15*	*3.58*	*113*	*39*	*17*	*52*	*69*
C+H_2O	*S=1/2*	*2.23*	*2.02*	*2.09*	*3.37*	*116*	*9*	*15*	*52*	*67*

Table 2

DFT calculated ionization energies for models

	Imidazole	Fluoride	Thiolate (Model A)	H-bonded Thiolate (Model B)
ΔE_{5C}	0.25	−0.99	−1.13	−0.81
ΔE_{6C}			−1.37	

Table 3

DFT calculated results for compound 0

		Geometry (distance in Å, angles in °)					Mulliken Spin			Covalency (%S_{3p})			$\Delta E_{syn-anti}$ (Kcal/mol)
		Fe-S	**Fe-O**	**O-O**	**Fe-N**	**O-O-S-C**	**Fe**	**S**	**OO**	**Π**	**Σ**	**total**	
A-OOH	Syn	2.37	1.85	1.45	2.03	0.3	1.00	0.07	0.11	10	33	43	−5.5
	Anti	2.47	1.84	1.45	2.03	79.5	1.02	0.00	0.13	0	29	29	
B-OOH	Syn	2.40	1.82	1.46	2.02	9.0	0.88	0.03	0.16	3	32	35	−2.5
	Anti	2.45	1.82	1.45	2.02	69.4	0.90	0.00	0.18	0	28	28	
C-OOH		2.39	1.83	1.45	2.03	47.8	0.95	0.05	0.11	5	32	37	

Table 4

Optimized geometric parameters for compound 0 (S=1/2), I (S=1/2) and ferryl (S=1) species with different axial ligands

Axial Ligand	Compound 0				Compound I			Ferryl		
(X)	Fe-N	Fe-X	Fe-O	O-O	Fe-N	Fe-X	Fe-O	Fe-N	Fe-X	Fe-O
Thiolate	2.03	2.35	1.84	1.45	2.02	2.68	1.61	2.03	2.48	1.65
Imidazole	2.02	2.13	1.78	1.44	2.02	2.13	1.63	2.02	2.20	1.62
F^-	2.03	1.80	1.83	1.46	2.02	1.82	1.65	2.03	1.83	1.65

Table 5

Relevant Mulliken spin densities for compound 0 (S=1/2), I (S=1/2) and ferryl (S=1) species with different axial ligands

Axial Ligand	Compound 0			Compound I			Ferryl		
(X)	Fe	X	OO	Fe	X	O	Fe	X	O
Thiolate	0.88	0.04	0.18	1.26	−0.95	0.81	1.29	−0.01	0.80
Imidazole	0.95	0.00	0.11	1.18	0.0	0.93	1.20	0.00	0.87
F^-	0.91	0.04	0.12	1.19	0.04	0.86	1.23	0.04	0.80

Table 6

Calculated ΔE's (Kcal/mol, PCM, ε=4.0) for compound 0 with different axial ligands

Axial Ligand (X)	$\Delta E_{protonation}$	$\Delta E_{O\text{-}O\ Heterolysis}$	$\Delta E_{O\text{-}O\ Homolysis}$	$\Delta E_{H\text{-}atom}$ ($C\text{-}H_{alkane}$)
Thiolate	−33	−46	+28	5.2
Imidazole	−9	−20	+26	5.8
F^-	−29	−40	+24	4.4

Table 7

DFT calculated energies (PCM, ε=4.0)

Axial ligand	BE_{O-H} (Kcal/mol)	Relative ΔBE_{O-H} (Kcal/mol)	Relative IE (Kcal/mol)	Relative E_{proton} (Kcal/mol)
$^{-}$SMe (Model B)	−96.3	0	0	0
Imidazole	−92.3	+4.0	−28.5	32.5
F^{-}	−97.5	−1.2	−8.0	6.8

Table 8

DFT optimized geometries and energies (PCM, ε = 4.0) for compound II

		Geometry	(distance in Å, angles in °)			Mulliken Spin			$\Delta E_{syn\text{-}anti}$ (Kcal/mol)	$\Delta E_{CompII\text{-}Fe(III)}$
		Fe-S/L	Fe-O	Fe-N	H-O-S-C	Fe	S/L	O		
A-OH	Syn	2.32	1.81	2.01	1.8	2.02	0.03	0.22	+1.5	30.4
	Anti	2.28	1.80	2.01	91.9	1.78	0.23	0.23		
B-OH	Syn	2.34	1.80	2.01	4.7	1.93	0.02	0.24	+0.8	30.5
	Anti	2.31	1.79	2.02	90.7	1.77	0.17	0.25		
F^-		1.74	1.77	2.02		1.82	0.12	0.17		29.8
Imidazole		2.07	1.78	2.02		0.86	−0.03	0.17		35.9